BNL-223620-2022-TECH
C-A/AP/666

Effective ZDC cross section derived from Vernier Scans during the RHICf run with polarized protons at 255 GeV in 2017

A. Drees

October 2022

Collider Accelerator Department
Brookhaven National Laboratory

U.S. Department of Energy
USDOE Office of Science (SC), Nuclear Physics (NP) (SC-26)

DISCLAIMER

Effective ZDC cross section derived from Vernier Scans during the RHICf run with polarized protons at 255 GeV in 2017

A. Drees

October 19, 2022

1 Introduction

At RHIC the collision rate per IP is measured by the Zero Degree Calorimeters (ZDC) [1]. The collision rate, as measured by the ZDC, corresponds to the rate of mutual forward neutral particles above a variable threshold and within a certain coincidence window. During run 17 the detector was operated for the RHICf experiment in a slightly different configuration from the earlier standard polarized proton run. Due to the different configuration the ZDC detector was calibrated for the rhicf setup by performing a set of dedicated vernier scans [2]. A total of 9 vernier scans were performed. This note presents the data and summarizes the results, i.e. effective ZDC cross section from those scans for the rhicf running period

2 Vernier Scan Technique

Table 1 lists the fills with vernier scans and the beam intensities. The fills had one, two or four scans. The transverse size and shape of the beam overlap region is measured by recording

fill	time	beam moved	$I_B[10^{11}]$	$I_Y[10^{11}]$	
21145	06/25, 12:58-13:16	B	92	74	
21148-1	06/26, 02:34-02:50	B	104	100	wfg error during scan
21148-2	06/26, 02:55-03:10	B	104	100	
21149-1	06/26, 10:47-11:01	Y	86	83	
21149-2	06/26, 15:52-16:08	B	85	82	
21150-1	06/27, 00:04-00:18	Y	104	105	
21150-2	06/27, 00:24-00:38	Y	104	105	
21150-3	06/27, 04:36-04:50	B	104	105	
21150-4	06/27, 05:35-05:49	Y	104	104	

Table 1: List of fills with vernier scans during the 2017 RHICf run. All scans were done with 111x111 filling patterns.

the interaction rate as a function of the transverse beam separation. A fit of the measured interaction rate as a function of the separation allows to determine the effective beam size, and thus the average emittance, as well as the maximum achievable collision rate and the effective cross section of the detector in use. Typically additional effects such as a possible crossing angle or the hourglass effect require correction factors to be applied. Beta-functions at the IP, β^*, were measured for the RHICf setup and β^* values of 7.3 m (H) and 7.2 m (V) were used in this note. The beam energy of 255 GeV corresponds to $\gamma = 271.6$.

2.1 The Fit Function

The shape of the overlap region, i.e. the collision rate $R_{coll}(x)$ as a function of distance between the two beams, x, is mapped by the vernier scan and can usually best be described by a single Gauss-function:

$$R_{\mathrm{coll}}(x) \;=\; R_{\mathrm{Bkgd}} \;+\; R_{\mathrm{max}} \;\times\; \exp\left(\frac{-(x-x_0)^2}{2\,\sigma_{\mathrm{x}}^{\mathrm{VS}}}\right) \tag{1}$$

with the 4 free parameters:
R_{Bkgd}: non-collision related background signal in the collision rate
R_{max}: maximum collision rate seen by the ZDC detector (corrected for background)
x_0: location of the maximum
σ_x: width of the overlap region
The application and DAQ software that supports fully automated vernier scans employs single-Gauss fits for its online analysis [3].

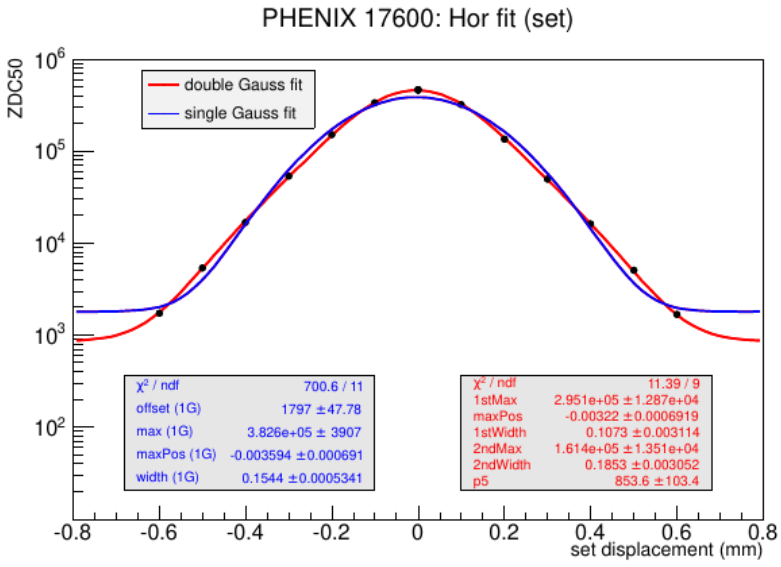

Figure 1: Horizontal data from a vernier scan in fill 17600 at the PHENIX experiment fitted with a 1-Gauss and a 2-Gauss fit function. The 2-Gauss fit function is clearly favored by about a factor 50 in χ^2/ndf

However, in the case of proton beams at 255 GeV, the single Gauss approach does no longer fit the data (as shown in Figure 1). The fit data shown here is fom RHIC run 13 (from fill 17600)

and was selected for demonstration purposes only. For these cases, a double Gauss-function is chosen:

$$R_{\rm coll}(x) \; = R_0 \; R_{\rm max,1} \; \times \; \exp\left(\frac{-(x-x_0)^2}{2\;\sigma^{\rm VS}_{\rm x,1}}\right) \; + \;\; R_{\rm max,2} \; \times \; \exp\left(\frac{-(x-x_0)^2}{2\;\sigma^{\rm VS}_{\rm x,2}}\right) \qquad (2)$$

The double Gauss function has 5 free parameters:
$R_{\rm max,1}$: maximum collision rate of the core region
x_0: location of both the maxima
$\sigma_{\rm x,1}$: width of the core overlap region
$R_{\rm max,2}$: maximum of the tail distribution
$\sigma_{\rm x,2}$: width of the tail region

The double Gauss approach is not needed to describe the data for protons at 100 GeV nor for Heavy Ions and its necessity was first observed during Run-9 [4]. During the RHICf run with the large β^* value the double Gauss approach is only mildly favored but chosen for consistency with the previous run and previous years. We assume that both Gauss distributions, core and tail, are centered around the same location x_0. All data from Run-17 was fitted with the double Gauss even in cases when the χ^2/ndf for the single Gauss fit was not quite as large as in Figure 1 and in the single digit range.

3 The Effective Cross Section

The effective detector cross section $\sigma^{\rm eff}_{\rm ZDC}$ of a detector, in this case the ZDCs, can be determined by the beam current, the collision rate and the overlap region $\sigma^{\rm VS}_{\rm x,y}$ of the two beams. The maximum collision rate and the width of the overlap region are derived from the fits to the vernier scan data.

$$\sigma^{\rm eff}_{\rm ZDC} = \frac{R_{\rm max}\; 2\pi \; n_B \; n_Y \; \sigma^{\rm VS}_{\rm x} \; \sigma^{\rm VS}_{y}}{n_{\rm coll} \; f_{\rm rev} \; N_B \; N_Y} \qquad (3)$$

where:
$R_{\rm max}$ = maximum collision rate seen by the ZDC detector (corrected for background)
$n_B,\; n_Y$ = number of blue and yellow bunches respectively
$\sigma^{\rm VS}_{\rm x,y}$ = RMS beam-overlap size, derived from the fit to the vernier scan data
$n_{\rm coll}$ = number of colliding bunch pairs in the IP where the ZDC detector is located
$f_{\rm rev}$ = revolution frequency, approx. 78.4 kHz
$N_{\rm B,Y}$ = total number of blue and yellow protons, from DCCT

Figure 2 shows one example of a vernier scan, here in the vertical plane in IP6, moving the yellow beam. The top graph depicts the ZDC coincidence rate as a function of the set value, i.e. based on the model, the bottom depicts the ZDC coincidence rate as a function of the measured distance of the two beams. Both are fitted with a double Gauss-function according to Equation 2. The χ^2/ndf in the top graph (using set values from the model) reaches 1.5 and is thus about half ot that in the bottom graph (using measured distances). This ratio is typical for the RHICf scans demonstrating that using the set displacements (i.e. data from model) yields better fit results. The beam overlap size $\sigma^{\rm VS}$ in Equation 3 is given by the combination of the

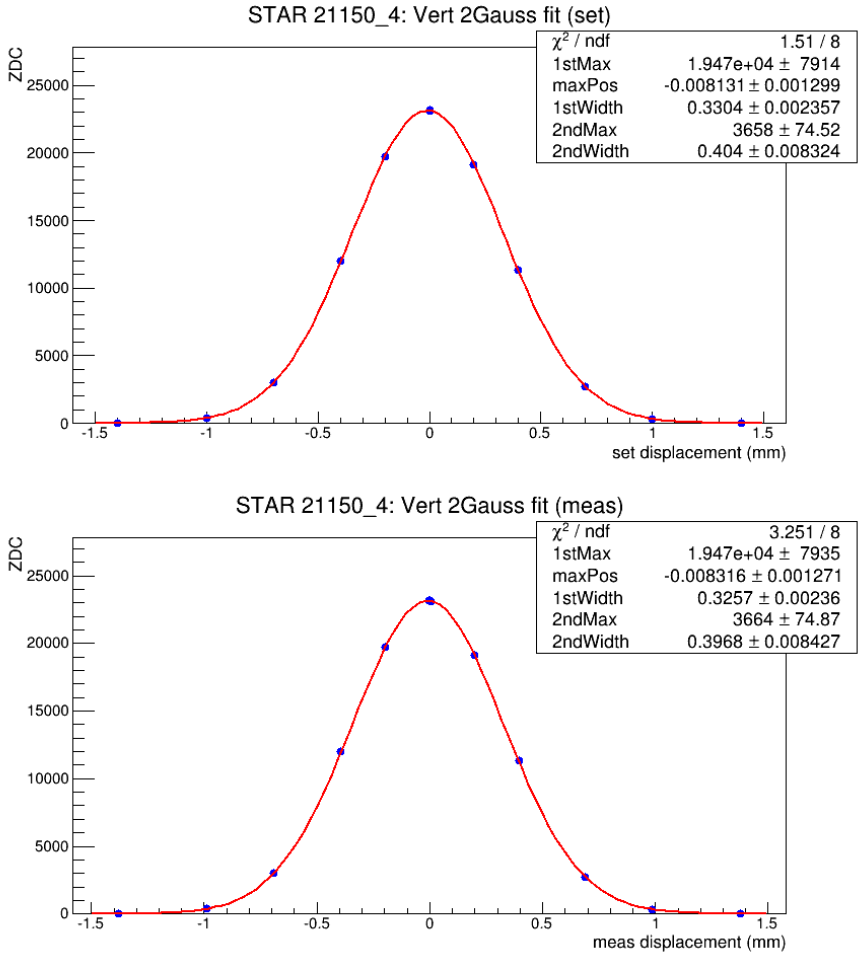

Figure 2: Vertical scan in fill 21150_4. The factor 2 difference in χ^2 between model (top) and measured (bottom) is typical for the RHICf scans.

two widths from the double Gauss fit. The combined width adds the two individual widths according to their amplitudes:

$$\sigma_{\mathrm{x,y}}^{\mathrm{comb}} = \sigma_1^{\mathrm{x,y}} \frac{R_{\mathrm{max},1}}{R_{\mathrm{max},1} + R_{\mathrm{max},2}} + \sigma_2^{\mathrm{x,y}} \frac{R_{\mathrm{max},2}}{R_{\mathrm{max},1} + R_{\mathrm{max},2}} \tag{4}$$

"x" and "y" refer to the two planes, while "1" and "2" refer to the core (1) and tail (2) part of the distribution respectively. Once the measured widths from the two approaches, using set or measured distances, are combined they agree within 15 μm.

Several corrections apply to the cross section and/or emittance measurement using the vernier scan method. They affect the collision rate (accidental coincidences), the beam current measurement (fill pattern and debunched beam) and the measurement of the width (hour-glass, crossing angle, beam-beam, model inaccuracy). The various effects are outlined below. However, the importance varies for different lattices and different species. For instance, there is practically no debunched beam present for protons and there is no need to not use the DCCT to measure the beam current.

3.1 Accidental Coincidences

The collision rate, defined by the ZDC coincidences, is contaminated by false, or accidental, coincidence signals caused by high singles rates. Singles rates, i.e. the signal from just one side of the ZDC detector, contain a large amount from the coincidence signal and an even larger portion of unrelated signals that are typically from collisions but not from mutually forward neutral particles. The signal from the blue-incoming side is referred to as $\mathrm{ZDC_B}$, and from the yellow-incoming side as $\mathrm{ZDC_Y}$. A purely statistical approach to correct for accidental coincidences yields:

$$\mathrm{ZDC_{BY}} = \frac{\mathrm{ZDC_B\ ZDC_Y\ n_{coll}}}{\mathrm{n_B\ n_Y}\ f_{\mathrm{rev}}} \tag{5}$$

$$\mathrm{ZDC_{corr}} = \mathrm{ZDC_{raw}} - \mathrm{ZDC_{BY}} \tag{6}$$

with the parameters equivalent to Equation 3 and $\mathrm{ZDC_{raw}}$ corresponding to the uncorrected collision rate. This approach overestimates the number of accidental coincidences by hits in the two sides of the ZDC detector that lead to coincidence hits but are not true beam crossing events. The following Equation corrects for multiple hits that are counted as a single hit and contains the correction for accidental hits from above [5]:

$$\mathrm{ZDC_{log.corr}} = \mathrm{n_{coll}}\ f_{\mathrm{rev}}\ \left(-ln\left(1 - \frac{\mathrm{ZDC_{raw}} - \mathrm{ZDC_{BY}}}{\mathrm{n_{coll}} f_{\mathrm{ref}} + \mathrm{ZDC_{raw}} - \mathrm{ZDC}_B - \mathrm{ZDC}_Y}\right)\right) \tag{7}$$

For the RHICf run in 2017 this correction is very small. Nevertheless, accidental collision rates are always taken into account and are subtracted from the measured raw coincidence rates for each data point.

4 Uncorrected Cross Section Results

The measured effective ZDC cross sections are summarized in Table 2 and shown in Figure 3. No corrections were applied other than accidental collision rates in the table as well as in the graph below. For the distance between the beams as measured by the BPMs only the BPMs of the moving ring were taken into account and interpolated to the IP in the center.

The cross section results are graphed in Fig. 3. The averaged cross section for the data set based on model is shown in the upper right corner with a χ^2/ndf of about 2.5. The combined cross section for the data set based on BPM measured distances has a χ^2/ndf of about x2 larger than that.

The two results differ by 2.7%. The model based result is going to be used in the following and the instantaneous luminosity quoted in Tab. 2 is based on the model values. While the measured effective cross sections within one fill agree well with each other there appears to be a larger scatter from fill to fill. This applies to both datasets but the scatter in the BPM based results is generally larger than in the model based one.

5 Corrections

Collision rates are always corrected for accidental coincidences (see above). This section deals with all other corrections.

fill	ring	model				BPM		
		$\sigma_{\rm eff}^{\rm ZDC}[mbarn]$	$\mathcal{L}[10^{31}cm^{-2}s^{-1}]$	$\sigma_x[\mu m]$	$\sigma_y[\mu m]$	$\sigma_{\rm eff}^{\rm ZDC}[mbarn]$	$\sigma_x[\mu m]$	$\sigma_y[\mu m]$
21145	B	2.440	0.669	335	321	2.413	336	316
21148-1	B					2.438	328	305
21148-2	B	2.496	1.048	328	322	2.442	328	308
21149-1	Y	2.404	0.707	335	315	2.298	326	310
21149-2	B	2.400	0.626	353	332	2.320	354	320
21150-1	Y	2.481	1.083	335	319	2.406	331	313
21150-2	Y	2.480	1.073	335	321	2.432	333	317
21150-3	B	2.479	0.951	353	339	2.409	353	331
21150-4	Y	2.491	0.927	359	342	2.387	350	337

Table 2: Effective cross sections and instantaneous luminosities during the RHICf vernier scans. Results based on model and measured distances (BPM) are included. Statistical error bars are between 0.7% and 0.9% and will be rounded to 1% for the effective cross section and instantaneous luminosity.

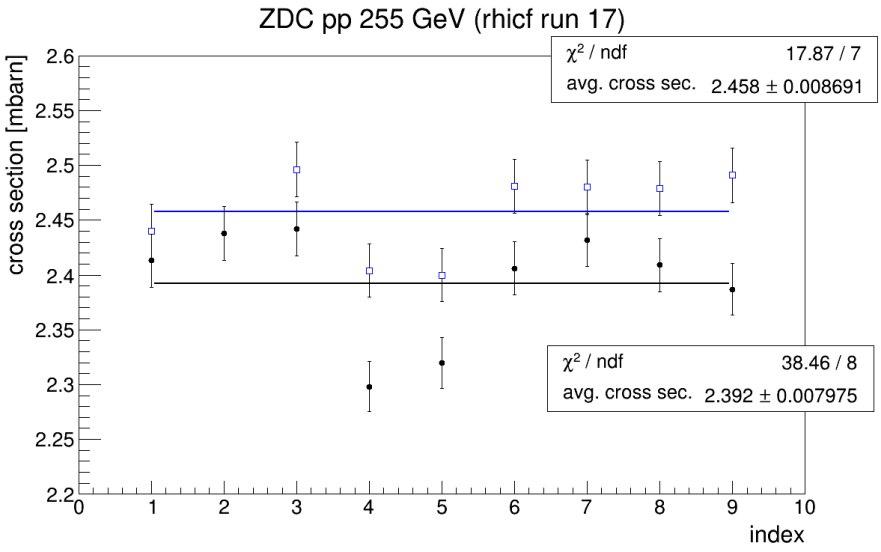

Figure 3: Effective cross section 2G fit results based on using the model (blue squares) and the measured distances (black dots). The fit results based on model are favored by about a factor 2 in χ^2/ndf. Error bars shown are statistical only (1%).

5.1 Beam Current and Fill Pattern

The collision rate, or rather the ZDC coincidence rate, is normalized to the beam intensity at the start of the scan point-by-point to address the slight change in beam current as the scan is progressing. For this correction the total circulating beam is used as measured by the DCCTs [6] while the measurements from the WCM [6] (total bunched beam) are ignored. This assumes that, with protons, all beam is bunched. While there is no ongoing debunching of proton beams during the store, beam could systematically debunch at the time of rebucketing. Systematic and small bunched beam loss is difficult to measure since there is a habitual discrepancy between the

WCM and the DCCT that changes when the WCM changes its gain setting (about 10 times per store) and the WCM measurement will change accordingly by up to 2% at times. Such automatic gain adjustments will also happen at the time of rebucketing. One cannot distinguish between a loss of bunched beam and the appearance of a change in beam current due to gain changes. Therefore the typical size of the change right after rebucketing is treated as a systematic error. For the stores with the vernier scans this virtual loss of bunched beam is small, $\leq 0.5\%$. The systematic error assigned to this effect is 0.5% and is assigned scan by scan since each collision rate measurement is normalized to the beam current at the start of each of the vernier scans.

In Equation 3 the beam current in each bunch is given as the total number of protons per ring divided by the number of bunches in blue and yellow respectively: $N_{\mathrm{total}}/\mathrm{n_{B,Y}}$, thus using an average bunch intensity. This approach relies on a uniform distribution of the total beam over the bunches in the rings. Large bunch intensity fluctuations could potentially change the actual product depending on the colliding pairs of bunches and their individual intensities.

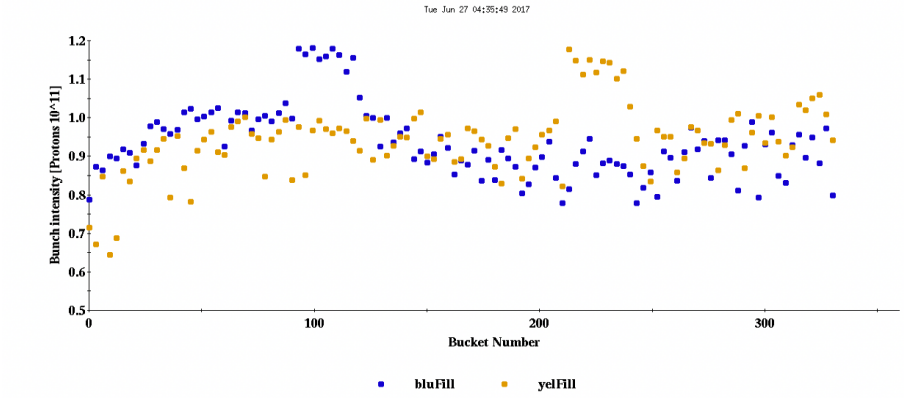

Figure 4: WCM measured bunch intensities for the blue and yellow beam during fill 21150.

Figure 4 shows the store with the largest fluctuations in the fill pattern (21150).

The graph shows the blue and yellow patterns respectively (blue and dark yellow dots) as they are lined up in IP8 and IP2, which is where the two abort gaps are aligned. To reflect the pairing in IP6 the blue bunch pattern is shifted by a third of the ring. In this particular case the actual product of the blue and yellow bunches would change by about 3% if paired correctly compared to assuming an average bunch intensity instead of the correct pairs. In order to take this into account, a correction factor has been computed for each of the four fill individually from the ratio of the product of the averaged bunch intensities over the product of the correctly paired bunch intensities. Tab. 3 lists the four fill pattern correction factors. There is only one

fill	correction factor
21145	1.0
21148	0.962
21149	1.007
21150	0.968

Table 3: Correction factors for the store to store fill pattern correction.

factor per store, not per scan, since the fill pattern cannot change during a store. The final

corrected cross sections are all corrected with this factor. Since we can correct for this effect, no additional systematic error is assigned although the bunch by bunch intensity measurement relies on the WCM. However, it is only used as a relative measurement and not as an absolute measurement. Therefore the rather large error stemming from the frequent gain changes and store to store variation does not enter.

5.2 Hourglass Reduction

The hourglass reduction factor $R_{\rm hg}$ [7] represents a loss in luminosity due to geometrical effects for Gaussian beams. The geometrical effect is caused by the parabolic shape of the beta-function along z in the IP between the triplet quadrupoles. For this note, $R_{\rm hg}$ was calculated using the "StoreAnalysis" application [8]. For the fills analyzed, this factor ranges from 0.990 to 0.995 for protons at 255 GeV in RHIC for the RHICf lattice used in run 17. The hourglass effect is depending on the bunch length (the longer the bunches the smaller the reduction factor i.e. the larger the potential effect). However, due to the distance of the ZDCs from the IP (20 m), this geometrical effect has no implication on the effective cross section for this particular detector. At this distance the beam size simply appears enlarged by the hourglass effect leading to a collision rate that is reduced but the true rate none-the-less. The measured effective cross section (see Eq. 3) is independent of the beta-function at the IP. The hourglass correction would need to be applied for emittance measurements though. The hourglass enlarged beam width, as seen by the ZDC detectors, has to be projected to the 'true' width at the IP with a known value of β^* to calculate the emittance. However, for this lattice this effect on the emittance measurement is very small and negligible.

5.3 BPMs

Beam position measurements rely on the BPMs [9], here in particular the DX BPMs which are attached to the DX magnets, approximately 8 m from the the Interaction Point (IP). DX BPMs are in a common beam pipe and subject to both beams.

5.3.1 Absolute Beam Position at the IP

Issues of the beam position measurement systematically affect the measurement of the beam width. There are two components: relative and absolute measurements. BPMs appear reliable and accurate when used for relative measurements (i.e. step size in a vernier scan, see 5.3.3).

Unfortunately, in absolute terms the beam position measurement is difficult and much less accurate. The position of the two beams at the IP, provided they are in optimized head-on collisions, should give the same value regardless of which beam is measured. In principle, there are two devices available to extrapolate to the IP, the DX BPMs and the Q1 BPMs. The distance between the Q1 BPMs is 50.05 m, and the distance between the DX BPMs is 16.32 m. There is only a drift between the DX BPMs but two horizontal dipoles (D0 and DX) between the two Q1 BPMs. DX BPMs have the extra difficulty - or advantage - that they are subject to both beams, hence any possible physical offset would apply to both beams and will thus cancel out when the difference between the two beams is calculated. The position of the beam at the IP for one beam (blue or yellow) is given by

$$\mathrm{Pos_{IP}} = \frac{1}{2}\left(\mathrm{BPM_{in}} + \mathrm{BPM_{out}}\right), \tag{8}$$

with "in" and "out" referring to the two sides of the IP (in-coming and out-going). The difference Δ between the two beams according to the two devices ("DX" or "Q1") is defined as follows:

$$\Delta_{\text{device}} = \text{Pos}_{\text{IP}}^{\text{blue}} - \text{Pos}_{\text{IP}}^{\text{yellow}}, \tag{9}$$

where Pos_{IP} is calculated according to Equation 8 above using either DX BPM or Q1 BPM. This is done for the two planes separately. The results are summarized in Table 4 below.

fill	$\Delta_{\text{DX}}^{\text{H}}$	$\Delta_{\text{Q1}}^{\text{H}}$	$\Delta_{\text{DX}}^{\text{V}}$	$\Delta_{\text{Q1}}^{\text{V}}$
21145	-45	-410	-30	1650
21148-1	-30	-415	-10	1630
21148-2	-30	-410	5	1615
21149-1	0	-415	60	1640
21149-2	5	-410	55	1655
21150-1	0	-405	0	1630
21150-2	20	-400	5	1640
21150-3	0	-410	15	1620
21150-4	0	-420	15	1630

Table 4: Measurements of the difference of the blue and yellow beam position at IP6 using DX and Q1 BPMs rounded to the nearest multiple of 5. Units are μm.

The problem with these numbers is apparent. Taking the DX BPM measurements alone, the blue and yellow beams are separated by up to 60 μm - while colliding head-on. Head-on collisions are guaranteed by the vernier scans and all data in Table 4 is taken right after a successful scan or just before but after an optimization. In addition, the "fake" separation is not constant but varies from store to store by a total of 90 μm (vertical plane) and 65 μm (horizontal plane). The uncertainty in the determination of the absolute beam position at the IP when using the DX BPM is as large as the largest measured "fake" separation, i.e. 90 μm. Using a larger sample of fills rather than the 4 fills with vernier scans, might reveal even larger pseudo separations.

Due to the size of the position discrepancy between the two beams, the Q1 BPMs were also consulted in hopes of reducing the uncertainty. The results are also listed in Table 4. The first observation is that the alleged difference between the two beams as measured by the Q1 BPMs appears to be even larger, more than 1.5 mm, and that in the vertical plane, the plane without further optical elements between the two devices. Additionally, there appears to be no correlation between the values from the Q1 BPMs and the DX BPMs. The Q1 BPMs are of no help in reducing the absolute uncertainty.

The accuracy of the absolute position measurement, however, is irrelevant when determining the stepsize (see 5.3.3) and thus the size of the overlap region of the two beams. In the 2017 RHICf run the pseudo separation is small compared to the scanned range ($\pm$ 2 mm) and even smaller than the smallest stepsize of 0.2 mm. The absolute position error applies only to determining collision angles and corresponds to approximatel 5 μrad in both planes.

5.3.2 Collision Angles

Crossing angles can reduce the maximum collision rate to varying degrees depending on the bunch length and size. In order to determine this angle, all four DX BPMs in each plane on either side of the IP have to provide reliable and accurate absolute beam position measurements. Unfortunately very few scans as a function of the crossing angle were ever performed and there is no such scan from Run-17. One angle scan per run (energy and species) is recommendable.

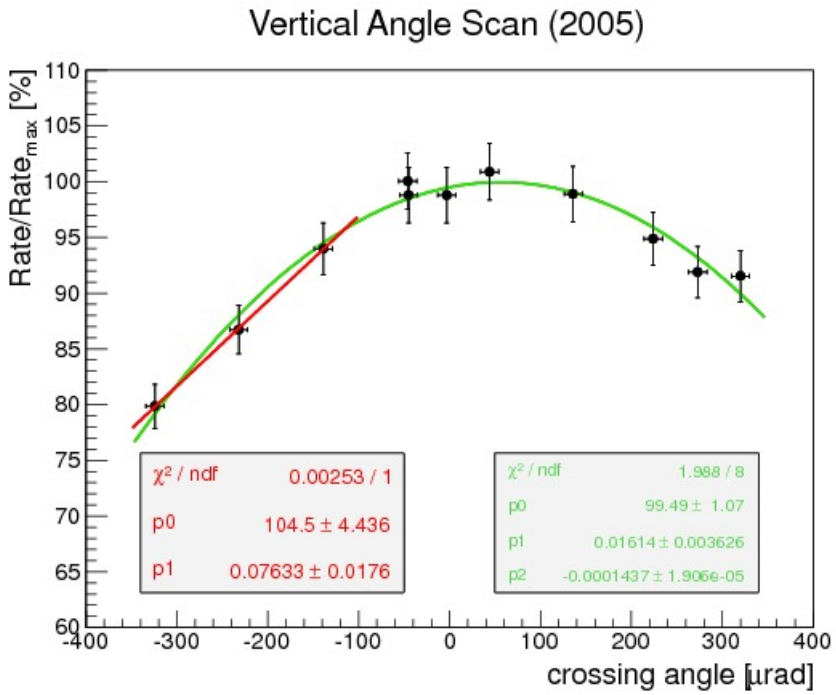

Figure 5: Relative change of collision rate in % as a function of the vertical crossing angle in IP8 in fill 7112 from Run-05.

However, the measurement procedure is delicate and the risk of creating large backgrounds or of losing the beam in the process is relatively large. One example covering a significant range of angles is shown in Fig. 5. The scan is from Run-5 and done with the yellow beam of polarized protons at 100 GeV. It is shown here just for the purpose of explaining the concept. The angle is measured using the yellow DX BPMs in the PHENIX IP. It turns out that in this particular case the measured "0" is off by only 60 μrads.

fill	21145	21148-1	21148-2	21149-1	21149-2	21150-1	21150-2	21150-3	21150-4
Hor DX	15	25	25	25	25	25	25	25	25
Vert DX	20	0	0	0	0	0	0	0	0

Table 5: Collision angles as measured by the DX BPMs and rounded to the nearest multiple of 5. Units are in μrad.

The scan covers a range of 0.7 mrad and is fitted with a parabola (green line and fit parameters). For comparison, an area at the 'shoulder' of the distribution is fitted with a straight line (red line and fit parameters). Even in this area, a few hundred μrad away from perfectly

aligned beams, the drop in the collision rate only corresponds to approximately 0.76 % per 10 μrad step.

As outlined in section 5.3.1 the Q1 BPMs are of no help in determining the collision angles. The measured collision angles using the DX BPMs are listed in Table 5.

The measured angles are all very small and have an uncertainty of 5 μrad (see 5.3.1 above). The DX data supports that the collision angles are very small ($\leq$ 30 μrad). Such a small angle is negligible, i.e. it has no visible effect on the luminosity, especially not when running with a large β^* of more than 7 m. Therefore, collision angles do not add an additional systematic uncertainty for the RHICf run.

5.3.3 Step size

For the 2017 RHICf run the beam position according to Eq. 1 and 2, is computed from the set value as well as the measured value (i.e. from the DX BPMs) when a vernier scan is performed. In order to study the reliability of the distance measurement, DX BPM data is compared to the set value from the model for each plane and ring for every individual vernier scan. Figure 6 shows one example.

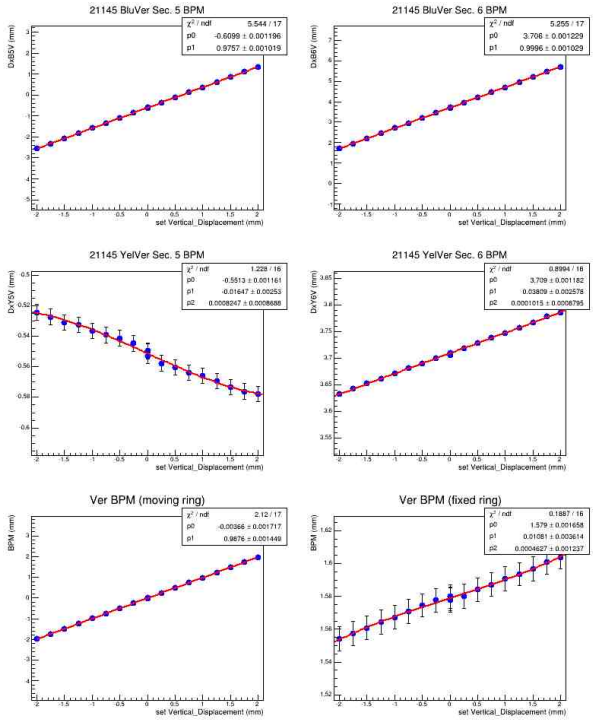

Figure 6: Distance between the two beams as measured by the DX BPMs as a function of the set value. The blue vertical scan shown here is from fill 21145.

The data shown is taken during the vertical vernier scan 21145. The top left and right graphs show the motion of the blue beam as seen by the DXB5V (left) and DXB6V (right) BPMs while the blue beam is moved across the yellow by a total of 4 mm. The center row shows the DX BPM measurements for the yellow, not moving beam. Since the blue beam was moved, the visible apparent "motion" of the yellow beam could be caused by the beam-beam effect or by electronic

fill	ring	Vert lin.	other [%]	Hor lin.	other [%]
21145	B	0.988	1.11	1.005	1.0
21148-1	B	-	-	-	-
21148-2	B	0.979	0.73	1.0	0.35
21149-2	B	0.966	0.96	1.001	0.66
21150-3	B	0.976	0.97	0.999	0.49
avg	B	0.977	0.94	1.001	0.63
21149-1	Y	0.987	2.27	0.979	0.27
21150-1	Y	0.987	2.17	0.985	0.18
21150-2	Y	0.986	2.03	0.991	0.13
21150-4	Y	0.985	2.17	0.978	0.08
avg	Y	0.986	**2.16**	0.983	0.17

Table 6: Linear correlation between measurements (DX BPMs) and set values (from model) for all RHICf scans. "other" specifies the range of motion seen in the DX BPMs of the not moving ring in percent of the total scanned region.

cross talk since the DX BPMs are subject to both beams. It is not possible to distinguish between the two effects. The bottom left and right graphs show the interpolated position measurement at the IP using Eq. 8 for the blue beam (left) and the yellow beam (right). In this particular case the blue DX BPMs as a function of the set values depict a fitted slope (p1) of 0.99. A slope of 1 would be perfect agreement between model and measurement. Simultaneously, the yellow beam appears to move by about 40 μm which corresponds to 1% of the total scanned region.

Tab. 6 summarizes the correlation between model and measured position for the blue scans (top rows) and the yellow scans (bottom rows). For scans where the blue beam was moved, model and measurement are in perfect agreement for the horizontal plane, and the measurement falls short by an average of 2% in the vertical plane. At the same time there appears about 1% of that motion in the other ring (vertical plane) or 6‰ in the horizontal plane. This is slightly different for measurements with the yellow BPMs where we see a consistent linear correlation of 98% in the horizontal plane with only 2‰ seen in the other ring and 99% in the vertical plane with 2% appearing in the other, not moving, ring. The store to store variation is small. We will correct the set stepsizes with the averaged linear correlation factor from Tab. 6 for the final value of the cross section. If the measurements of the non-moving beam were solely caused by beam-beam it would be implausible that it be consistently different for the two planes and rings. Therefore this is most likely electronic cross talk or a superposition of both effects. To address the uncertainty of motion of the non-moving beam, a systematic error of 2.2% is added. This is a conservative estimate based on the largest measured motion seen in the "other", non-moving, ring during a scan (see highlighted value in Tab. 6, bottom row).

6 Cross Section Final Results

The fully corrected effective ZDC cross sections are summarized and listed in Tab. 7. Here, all applicable corrections that were discussed above were taken into account. These values and the individual point by point errors of 1.5% are depicted in Fig. 7. The resulting effective cross section and error is calculated as the average and standard deviation of the individual cross sec-

fill	21145	21148-2	21149-1	21149-2	21150-1	21150-2	21150-3	21150-4
$\sigma_{\rm eff}^{\rm ZDC}[mbarn]$	2.391	2.353	2.349	2.368	2.330	2.329	2.351	2.339

Table 7: Fully corrected effective ZDC cross sections. Individual errors, statistical and beam current normalization, are 1.5%

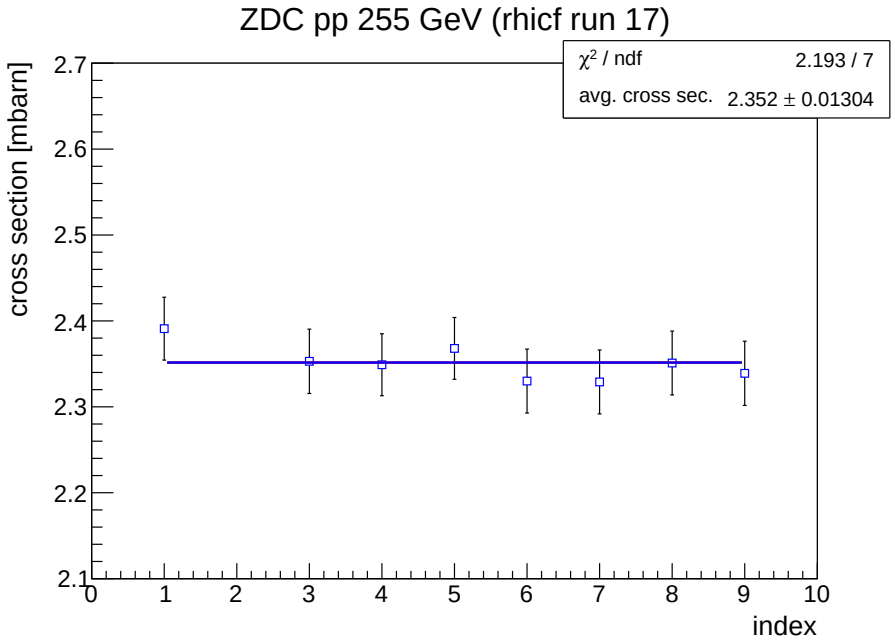

Figure 7: Cross sections calculated from corrected set values with point by point statistical and beam current measurement errors. Corrections included are BPM measured beam distances as well as fill pattern corrections.

tions summarized in the table above. Including the systematic error discussed in section 5.3.3 this yields:

$$\sigma_{\rm eff}^{\rm ZDC} = 2.351 \pm 0.021 \text{ (std. dev.) } \pm 0.052 \text{ (syst.) mbarn}$$

References

[1] A. Baltz et al., Nucl. Instr. and Methods, A417 (1998) 1.

[2] S. Van Der Meer, ISR-PO/68-31, KEK68-64.

[3] Ted d'Ottavio, A. Drees, http://www.cadops.bnl.gov/Controls/doc/lisa/lisa.html

[4] K.A.Drees (BNL), S. White (CERN), "Vernier Scan Results from the First RHIC Proton Run at 250 GeV", IPAC10 Proceedings, 2010.

[5] D. Cronin-Hennessy, A. Beretvas and P.F. Derwent, "Luminosity monitoring and measurement at CDF", Nucl. Instruments and Methods A433 (2000) 37

[6] http://www.cadops.bnl.gov/Instrumentation/InstWiki/index.php/RHIC_Current_Transformer

[7] M.A. Furman, "Hourglass Effects for Asymmetric Colliders", PAC Proceedings, 1991.

[8] StoreAnalysis application, S. Binello, W. Fischer, private communication

[9] R. Michnoff et al., "RHIC BPM SYSTEM AVERAGE ORBIT CALCULATIONS", PAC proceedings, 2009.